2024 IEEE 63rd Conference on Decision and Control (CDC)
December 16-19, 2024. MiCo, Milan, Italy

# Consistent Rigid Body Localization from Range Measurements with Anchor Position Uncertainty

Hongxu Zhao[1], Guangyang Zeng[1,2], Hongdong Jiang[1], Xiaoqiang Ren[3], Wen Yang[4] and Junfeng Wu[1]

***Abstract*— Rigid Body Localization (RBL) using range measurements has recently attracted much attention. In some large and complicated scenarios, we may not obtain the accurate positions for anchors deployed in the environment. However, few works have considered the anchor position uncertainty. In this paper, we formulate the Maximum Likelihood (ML) RBL problem with anchor position uncertainty and find that the ML estimate is not necessarily consistent. As an alternative, we propose a two-step estimator MGN-CULS, which is both consistent and computationally efficient. In the first step, we develop a closed-form initial estimate with consistency using bias-eliminating techniques. In the second step, we design a modified Gauss-Newton iteration to refine the initial estimate without destabilizing the consistency. Simulation results demonstrate the stable and accurate performance of our proposed algorithm.**

## I. INTRODUCTION

Traditional source localization refers to estimating the position of the source in a specific coordinate system. In recent years, Rigid Body Localization (RBL) has attracted widespread attention, which involves estimating both the position and orientation of a rigid body [1]–[3]. It serves as a key technology in many applications, ranging from robot positioning and navigation [4], augmented reality [5] to 3D reconstruction [6].

RBL generally relies on measurements between sensor tags installed on a rigid body and anchor points with known global positions. Range measurement is a commonly used measurement type for RBL [7]–[9]. Under the i.i.d. Gaussian noise assumption, the Maximum Likelihood (ML) formulation of the range-based RBL is a constrained least-squares problem [10]–[12]. Its nonlinearity and nonconvexity make it challenging to solve, and a commonly used method is relaxing it into a Squared Least-Squares (SLS) problem. Chepuri *et al.* [10] introduced a modification to the SLS problem by projecting squared measurements onto the null space of unit vectors. Chen *et al.* [11], leveraged the structure of the rotation matrix, introducing a Generalized Trust Region Subproblem (GTRS). Jiang *et al.* [12] transformed the original problem into a linear one, obtaining a consistent closed-form solution, and further enhancing accuracy through a single Gauss-Newton iteration.

The above works assume the positions of anchors are noise-free, and only the range measurement noise is considered. However, in real scenarios, the anchor positions are obtained via some measurement methods, e.g., GPS and motion capture systems, which contain uncertainty. As far as we know, there exists some literature studying the range-based source localization with sensor position uncertainty [13]–[16], while the investigation on the calibration-free range-based RBL with anchor position uncertainty is still an open problem.

In this paper, we consider RBL using range measurements with anchor position uncertainty. We take both the anchor positions and rigid body pose as optimization variables to formulate the ML estimate and analyze the property of the ML estimate. We mainly focus on proposing a consistent estimate, which can converge to the true pose in probability as the anchor number increases.

We summarize our contributions as follows:

($i$). We formulate the range-based ML RBL problem with anchor position uncertainty and prove that the ML estimate is not necessarily consistent by presenting a counterexample.

($ii$). We design an asymptotically unbiased and consistent closed-form RBL estimator based on an elaborate bias elimination method.

($iii$). We refine the initial consistent estimate with a modified one-step Gauss-Newton iteration that can maintain the consistent property.

**Notations:** For a vector $\mathbf{x} \in \mathbb{R}^n$, $[\mathbf{x}]_i$ presents the $i$-th element of $\mathbf{x}$. For two vectors $\mathbf{x}$ and $\mathbf{y}$, $[\mathbf{x};\mathbf{y}] = [\mathbf{x}^\top, \mathbf{y}^\top]^\top$. For a matrix $\mathbf{A}$, $\mathrm{vec}(\mathbf{A})$ yields a vector by concatenating the columns of $\mathbf{A}$. For a quantity $\mathbf{x}$ corrupted by anchor position noise, we use $\mathbf{x}^o$ to denote its noise-free counterpart. Let $p = \{p_i\}_{i\in\mathbb{N}}$ and $q = \{q_i\}_{i\in\mathbb{N}}$ be two sequences of real numbers. If $t^{-1}\sum_{i=1}^t p_i q_i$ converges to a real number its limit $\langle p,q\rangle_t$ will be called the tail product of $p$ and $q$. We call $\|p\|_t = \sqrt{\langle p,p\rangle_t}$, if it exists, the tail norm of $p$. The notation $X_m = O_p(a_m)$ means that the set of values $X_m/a_m$ is stochastically bounded, i.e., for any $\varepsilon > 0$, there exists a finite $M$ and a finite $N$ such that for any $m > M$, $\mathbb{P}(|X_m/a_m| > N) < \varepsilon$.

## II. PROBLEM FORMULATION

We focus on the RBL problem with only the position uncertainty of anchors and discuss both the two-dimensional ($n = 2$) and three-dimensional ($n = 3$) cases.

[1]: School of Data Science, the Chinese University of HongKong, Shenzhen, Shenzhen, P. R. China, hxzsimon99@gmail.com, zengguangyang@cuhk.edu.cn, haodongjiang@link.cuhk.edu.cn, junfengwu@cuhk.edu.cn. [2]: Department of Automation, University of Science and Technology of China, Hefei, P. R. China. [3]: School of Mechatronic Engineering and Automation, Shanghai University, Shanghai, P. R. China, xqren@shu.edu.cn [4]:School of Information Science and Engineering, East China University of Science and Technology, Shanghai, P. R. China, weny@ecust.edu.cn.

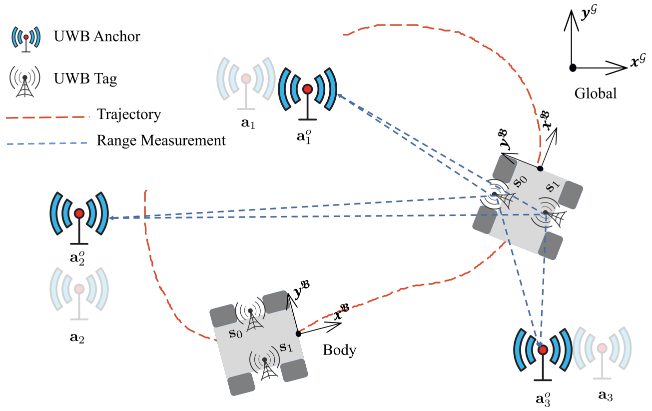


Fig. 1. Planar pose estimation from range measurements with anchor position uncertainty.

As tags are mounted on the rigid body, their position uncertainty is often small enough to be ignored compared with the range measurement errors, while anchors are placed in the global environment, making it much more difficult to obtain accurate positions, especially in some large and complicated situations. An example of a planar scenario is shown in Fig. 1. $M$ range measurement anchors (simplified as anchors in later paragraphs) are placed in the environment and $N$ range measurement tags (simplified as tags in later paragraphs) are placed on the rigid body. Let ${}^{\mathcal{G}}\mathbf{a}_m^o \in \mathbb{R}^n$ represent the fixed and accurate global position of the $m$-th anchor. The measured global position of the $m$-th anchor with uncertainty has the form

$$ {}^{\mathcal{G}}\mathbf{a}_m = {}^{\mathcal{G}}\mathbf{a}_m^o + \boldsymbol{\varepsilon}_m, \tag{1} $$

where $\boldsymbol{\varepsilon}_m \in \mathbb{R}^n$ denotes the position measurement noise. We denote ${}^{\mathcal{B}}\mathbf{s}_i \in \mathbb{R}^n$ as the fixed and accurate position of the $i$-th tag in the rigid body frame and assume it can be obtained exactly. Let $\mathbf{R}^o$ and $\mathbf{t}^o$ represent the pose of the rigid body in the global frame. For the sake of simplicity, in the following, we abbreviate ${}^{\mathcal{G}}\mathbf{a}_m$, ${}^{\mathcal{G}}\mathbf{a}_m^o$ and ${}^{\mathcal{B}}\mathbf{s}_i$ as $\mathbf{a}_m$, $\mathbf{a}_m^o$ and $\mathbf{s}_i$, respectively. The range measurement model with anchor position error is

$$ d_{im} = \|(\mathbf{a}_m - \boldsymbol{\varepsilon}_m) - \mathbf{R}^o\mathbf{s}_i - \mathbf{t}^o\| + r_{im}, \tag{2} $$

where $r_{im}$ is the range measurement noise.

Next, we list several assumptions of this work.

*Assumption 1:* The range measurement noises $r_{im}$'s are i.i.d. Gaussian noises with zero mean and known variance $\sigma^2 < \infty$. The anchor position noises $\boldsymbol{\varepsilon}_m$'s are i.i.d. Gaussian noises with zero mean and known covariance $\sigma_a^2\mathbf{I}_n$, where $\sigma_a^2 < \infty$. In addition, the range measurement noises and anchor position noises are independent.

*Assumption 2:* For the two-dimensional planer case ($n = 2$), there exist at least two tags and three non-colinear anchors. For the three-dimensional case ($n = 3$), there exist at least three non-colinear tags and four non-coplanar anchors. There is a range measurement $d_{im}$ between every pair of tag and anchor, for $i = 1 \ldots N$ and $m = 1 \ldots M$.

*Assumption 3:* The sample distribution $F_m$ of the sequence $\mathbf{a}_1^o, \mathbf{a}_2^o, \ldots$ converges to some distribution $F_\mu$, and denote the probability measure induced from $F_\mu$ as $\mu$.

*Assumption 4:* In the asymptotic case, there does not exist any line (any plane) $\mathscr{L}$ such that $\mu(\mathscr{L}) = 1$ for $n = 2$ ($n = 3$).

### A. ML estimator and consistency

In general, the ML estimator is quite important for its consistency and asymptotic efficiency. In other words, the ML estimate can converge to the true value with minimum variance in most cases. However, in the range-based RBL with anchor position uncertainty, we interestingly find out that the ML estimate cannot converge to the true value, which means that the ML estimator loses its consistency.

Motivated by works studying range-based source localization with sensor position uncertainty [17], we first formulate the following ML RBL problem considering anchor position uncertainty:

$$ \begin{aligned} \min_{\mathbf{P},\mathbf{R},\mathbf{t}} \; & \frac{1}{MN}\Big(\sum_{i=1}^{N}\sum_{m=1}^{M}\frac{(d_{im} - \|\mathbf{p}_m - \mathbf{R}\mathbf{s}_i - \mathbf{t}\|)^2}{\sigma^2} + \sum_{m=1}^{M}\frac{\|\mathbf{a}_m - \mathbf{p}_m\|^2}{\sigma_a^2}\Big) \\ \text{s.t.} \quad & \mathbf{R} \in \mathrm{SO}(n), \quad \mathbf{t} \in \mathbb{R}^n, \quad \mathbf{P} \in \mathbb{R}^{n\times M}, \end{aligned} \tag{3} $$

where $\mathbf{P} = [\mathbf{p}_1, \cdots, \mathbf{p}_M] \in \mathbb{R}^{n\times M}$ denotes the estimated anchor positions. Set $\mathbf{A} = [\mathbf{a}_1, \cdots, \mathbf{a}_M] \in \mathbb{R}^{n\times M}$ as the anchor position measurements and $\mathbf{d} = [d_{11}, \cdots, d_{NM}]^\top \in \mathbb{R}^{NM}$.

An optimal solution to the ML problem (3) is called the ML estimate and denoted as $\hat{\mathbf{P}}^{\mathrm{ML}}$, $\hat{\mathbf{R}}^{\mathrm{ML}}$, $\hat{\mathbf{t}}^{\mathrm{ML}}$. In the range-based RBL without anchor position uncertainty, under Assumptions 1-4, the ML estimate is consistent and asymptotically efficient [12]. However, the ML estimate to problem (3) is not necessarily consistent.

*Theorem 1:* The ML estimate is not necessarily consistent. In other words, as the anchor number $M$ increases, $\hat{\mathbf{R}}^{\mathrm{ML}}$ and $\hat{\mathbf{t}}^{\mathrm{ML}}$ may not converge to $\mathbf{R}^o$ and $\mathbf{t}^o$.

*Proof:* We prove this by presenting a counterexample. We simulate a planar situation in which all anchors are randomly placed inside a 100m $\times$ 100m room, and two tags are placed at $[0, 5]^\top$ and $[5, 5]^\top$ in the rigid body local frame. The noise level for range measurements is $\sigma = 1$ and the uncertainty level for anchor positions is $\sigma_a = 5$. The rigid body is located at $[5, 5]^\top$ and the rotation angle is at $60^o$. We run 10 Monte-Carlo experiments and present the average cost results.

In terms of the ML problem (3), based on the first-order optimality condition, we can obtain the optimal $\mathbf{P}$ as a function of $\mathbf{R}$ and $\mathbf{t}$, denoted as $\mathbf{P}^*(\mathbf{R}, \mathbf{t})$. On the one hand, we substitute the true pose $\mathbf{R}^o$, $\mathbf{t}^o$ and $\mathbf{P}^*(\mathbf{R}^o, \mathbf{t}^o)$ into the ML objective function. On the other hand, we take $\mathbf{R}^o$, $\mathbf{t}^o$ and $\mathbf{P}^*(\mathbf{R}^o, \mathbf{t}^o)$ as initial values and apply the Gauss-Newton method to seek a local minimum of the ML objective function. The two cost values are shown in Fig. 2. We observe that the cost gap between the true pose and the Gauss-Newton refined estimate converges to a fixed non-zero quantity as the anchor number increases. This result implies that the true pose is not a local minimum even in the large sample case, and indicates that the ML estimate is not consistent.

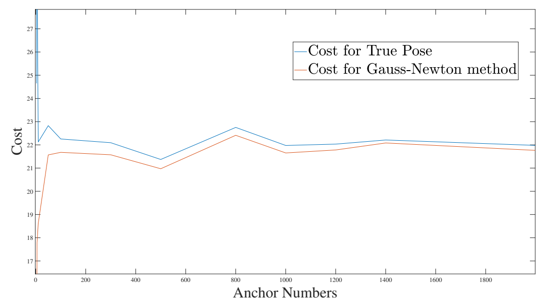


Fig. 2. Cost comparison.

■

### B. Cramér-Rao lower bound analysis

Denote the ground truth of parameters as $\mathbf{\Omega}^o = [\mathrm{vec}(\mathbf{R}^o);\mathbf{t}^o;\mathrm{vec}(\mathbf{A}^o)]$, we write the log-likelihood function as follows:

$$
\begin{aligned}
l(\mathbf{A},\mathbf{d};\mathbf{\Omega}^o) = &\sum_{m=1}^{M}(-\frac{\|\mathbf{a}_m-\mathbf{a}_m^o\|^2}{2\sigma_a{}^2}+\log\frac{1}{\sqrt{(2\pi)^n}\sigma_a^n}) \\
&+\sum_{i=1}^{N}\sum_{m=1}^{M}(-\frac{(d_{im}-\mu_{im})^2}{2\sigma^2}+\log\frac{1}{\sqrt{2\pi}\sigma}),
\end{aligned}
$$

where $\mu_{im} = \|\mathbf{a}_m^o-\mathbf{R}^o\mathbf{s}_i-\mathbf{t}^o\|$.

Then, we obtain the Fisher Information Matrix (FIM) by

$$
\mathbf{F} = \mathbb{E}\left\{\frac{\partial l(\mathbf{A},\mathbf{d};\mathbf{\Omega}^o)}{\partial\mathbf{\Omega}^o}\left(\frac{\partial l(\mathbf{A},\mathbf{d};\mathbf{\Omega}^o)}{\partial\mathbf{\Omega}^o}\right)^\top\right\}.
$$

The involved derivative can be written as

$$
\frac{\partial l(\mathbf{A},\mathbf{d};\mathbf{\Omega}^o)}{\partial\mathbf{\Omega}^o} = \begin{bmatrix}\dfrac{\partial l(\mathbf{A},\mathbf{d};\mathbf{\Omega}^o)}{\partial\mathrm{vec}(\mathbf{R}^o)}\\ \dfrac{\partial l(\mathbf{A},\mathbf{d};\mathbf{\Omega}^o)}{\partial\mathbf{t}^o}\\ \dfrac{\partial l(\mathbf{A},\mathbf{d};\mathbf{\Omega}^o)}{\partial\mathrm{vec}(\mathbf{A}^o)}\end{bmatrix},
$$

and

$$
\begin{aligned}
\frac{\partial l(\mathbf{A},\mathbf{d};\mathbf{\Omega}^o)}{\partial\mathrm{vec}(\mathbf{R}^o)} &= \sum_{i=1}^{N}\sum_{m=1}^{M}\frac{(d_{im}-\mu_{im})(\mathbf{s}_i\otimes\mathbf{I}_n)(\mathbf{a}_m^o-{}^{\mathscr{G}}\mathbf{s}_i)}{\sigma^2\|\mathbf{a}_m^o-{}^{\mathscr{G}}\mathbf{s}_i\|},\\
\frac{\partial l(\mathbf{A},\mathbf{d};\mathbf{\Omega}^o)}{\partial\mathbf{t}^o} &= \sum_{i=1}^{N}\sum_{m=1}^{M}\frac{(d_{im}-\mu_{im})(\mathbf{a}_m^o-{}^{\mathscr{G}}\mathbf{s}_i)}{\sigma^2\|\mathbf{a}_m^o-{}^{\mathscr{G}}\mathbf{s}_i\|},\\
\frac{\partial l(\mathbf{A},\mathbf{d};\mathbf{\Omega}^o)}{\partial\mathbf{a}_m^o} &= \sum_{i=1}^{N}-\frac{(d_{im}-\mu_{im})(\mathbf{a}_m^o-{}^{\mathscr{G}}\mathbf{s}_i)}{\sigma^2\|\mathbf{a}_m^o-{}^{\mathscr{G}}\mathbf{s}_i\|}+\frac{\mathbf{a}_m-\mathbf{a}_m^o}{\sigma_a^2}.
\end{aligned}
$$

where ${}^{\mathscr{G}}\mathbf{s}_i = \mathbf{R}^o\mathbf{s}_i+\mathbf{t}^o$.

To account for constraints of the rotation matrix, the constrained Cramér-Rao Lower Bound (CRLB) is given by

$$
\mathrm{CRLB} = \mathbf{U}(\mathbf{U}^\top\mathbf{F}\mathbf{U})^{-1}\mathbf{U}^\top,
$$

where the matrix $\mathbf{U}$ is related to the $\mathrm{SO}(n)$ constraint and is derived in [12] for $n=2$ and [18] for $n=3$. In simulations, we use the trace of the CRLB as a lower bound and present it along with the RMSE of different estimators.

## III. A Consistent Two-Step Estimator

In this section, we first propose a consistent estimator for the rigid body pose. Then, we devise a one-step Gauss-Newton iteration that can refine the initial consistent solution while maintaining the consistent property. Before that, we give the definition of a $\sqrt{M}$-consistent estimate, which is frequently used in this section.

*Definition 1:* Suppose $\hat{\mathbf{y}}$ is an estimate of $\mathbf{y}^o$. If $\hat{\mathbf{y}} = \mathbf{y}^o + O_p(1/\sqrt{M})$, then we call $\hat{\mathbf{y}}$ a $\sqrt{M}$-consistent estimate of $\mathbf{y}^o$. It has two meanings: First, the estimate $\hat{\mathbf{y}}$ converges to $\mathbf{y}^o$ as $M$ increases; Second, the convergence speed is $1/\sqrt{M}$.

For the sake of simplicity, in the rest of this paper, we use the notation $\approx$ to denote that the difference between two variables is in the order of $O_p(1/\sqrt{M})$. In other words, $\hat{\mathbf{y}}\approx\mathbf{y}^o$ implies $\hat{\mathbf{y}} = \mathbf{y}^o+O_p(1/\sqrt{M})$.

### A. Initial Consistent Estimator

First, we consider the model of range measurements without position uncertainty:

$$
d_{im} = \|\mathbf{a}_m^o-\mathbf{R}^o\mathbf{s}_i-\mathbf{t}^o\|+r_{im}. \tag{4}
$$

Let $\theta^o\in\mathbb{R}$ for $n=2$ ($\boldsymbol{\theta}^o\in\mathbb{R}^3$ for $n=3$) denote the rotation angle vector of the rigid body. Following the procedure in [12], we can obtain a closed-form solution

$$
\hat{\mathbf{y}}^{\mathrm{B}} = (\mathbf{H}^{o\top}\mathbf{H}^o)^{-1}\mathbf{H}^{o\top}\bar{\mathbf{d}}^o, \tag{5}
$$

where $\hat{\mathbf{y}}^{\mathrm{B}} = [\hat{\mathbf{x}}^{\mathrm{B}};\hat{\mathbf{t}}^{\mathrm{B}}]$, $\mathbf{H}^o = [\mathbf{H}_1^o,\mathbf{H}_2^o]$, $\mathbf{H}_1^o = -2(\mathbf{S}^\top\otimes\bar{\mathbf{A}}^{o\top})\mathbf{\Gamma}$, $\mathbf{H}_2^o = -2\mathbf{1}_N\otimes\bar{\mathbf{A}}^{o\top}$, $\bar{\mathbf{A}}^o = \mathbf{A}^o\mathbf{P}$, $\mathbf{S} = [\mathbf{s}_1\ \mathbf{s}_2\cdots\mathbf{s}_N]$, $\mathbf{P} = \mathbf{I}_M-(\mathbf{1}_M\mathbf{1}_M^\top)/M$,

$$
\tilde{\mathbf{d}}^o = \begin{bmatrix}\tilde{d}_{11}^o & \cdots & \tilde{d}_{N1}^o\\ \vdots & \ddots & \vdots\\ \tilde{d}_{1M}^o & \cdots & \tilde{d}_{NM}^o\end{bmatrix},
$$

$\tilde{d}_{im}^o = d_{im}^2-\|\mathbf{a}_m^o\|^2-\sigma^2$, and $\bar{\mathbf{d}}^o = (\mathbf{I}_N\otimes\mathbf{P})\,\mathrm{vec}(\tilde{\mathbf{d}}^o)$.

For the planar situation ($n$=2), $\hat{\mathbf{x}}^{\mathrm{B}} = [\sin\hat{\theta}^{\mathrm{B}};\cos\hat{\theta}^{\mathrm{B}}]$ and

$$
\mathbf{\Gamma} = \begin{bmatrix}0 & 1 & -1 & 0\\ 1 & 0 & 0 & 1\end{bmatrix}^\top.
$$

For the 3-D situation ($n$=3), the rotation matrix $\hat{\mathbf{R}}^{\mathbf{B}}$ can be written as

$$
\hat{\mathbf{R}}^{\mathbf{B}} = \begin{bmatrix}x_1 & x_4 & x_7\\ x_2 & x_5 & x_8\\ x_3 & x_6 & x_9\end{bmatrix},
$$

and $\hat{\mathbf{x}}^{\mathrm{B}} = [x_1,x_2,x_3,x_4,x_5,x_6,x_7,x_8,x_9]^\top$, $\mathbf{\Gamma} = \mathbf{I}_9$.

*Theorem 2 (Theorem 2 [12]):* Under Assumptions 1-4, the estimate $\hat{\mathbf{y}}^{\mathrm{B}}$ is $\sqrt{M}$-consistent, i.e., $\hat{\mathbf{y}}^{\mathrm{B}}\approx\mathbf{y}^o$.

Equation (5) provides a consistent estimate for the problem without anchor position uncertainty as stated in [12]. However, in our problem, we cannot obtain the precise position $\mathbf{a}_m^o$. Directly replacing $\mathbf{a}_m^o$ with $\mathbf{a}_m$ will introduce uncertainty into the $\mathbf{H}$ term. As we obtain estimate $\hat{\mathbf{y}}$ using $\dfrac{\mathbf{H}^\top\mathbf{H}}{MN}$ and $\dfrac{\mathbf{H}^\top\bar{\mathbf{d}}}{MN}$, noises in those two terms appear in quadratic form, which will bring bias in estimating $\hat{\mathbf{y}}$. Hence, we design a consistent estimator that estimates the bias-eliminated estimate $\hat{\mathbf{y}}$ which eliminates the bias caused by anchor position uncertainty:

$$\hat{\mathbf{y}} = \left(\frac{\mathbf{H}^\top\mathbf{H}-\mathbf{G}_{a1}}{MN}\right)^{-1}\left(\frac{\mathbf{H}^\top\bar{\mathbf{d}}-\mathbf{G}_{a2}}{MN}\right), \tag{6}$$

where $\mathbf{H}$ and $\bar{\mathbf{d}}$ are defined by replacing $\mathbf{a}_m^o$ with $\mathbf{a}_m$ in $\mathbf{H}^o$ and $\bar{\mathbf{d}}^o$, respectively, and

$$\mathbf{G}_{a1} = 4KM\sigma_a^2\begin{bmatrix}\mathbf{G}_{a11} & \mathbf{G}_{a12}\\ \mathbf{G}_{a13} & \mathbf{G}_{a14}\end{bmatrix},\ \mathbf{G}_{a2} = 4K{\sigma_a}^2\begin{bmatrix}\mathbf{G}_{a21}\\ \mathbf{G}_{a22}\end{bmatrix},$$

$$\mathbf{G}_{a11} = \mathbf{\Gamma}^\top(\mathbf{S}\mathbf{S}^\top\otimes\mathbf{I}_n)\mathbf{\Gamma},\ \mathbf{G}_{a12}=\mathbf{\Gamma}^\top(\mathbf{S}\mathbf{1}_N\otimes\mathbf{I}_n),\ \mathbf{G}_{a13}=\mathbf{G}_{a12}^\top,$$
$$\mathbf{G}_{a14} = N\mathbf{I}_n,\ \mathbf{G}_{a21} = \mathbf{\Gamma}^\top(\mathbf{S}\mathbf{1}_N\otimes\mathbf{A}\mathbf{1}_M),\ \mathbf{G}_{a22} = N\mathbf{A}\mathbf{1}_M.$$

*Lemma 1 ( [19, Lemma 4]):* Let $\{X_k\}$ be a sequence of independent random variables with $\mathbb{E}[X_k]=0$ and $\mathbb{E}\left[{X_k}^2\right]\le\varphi<\infty$ for all $k$. Then, there holds $\sum_{k=1}^M X_k/M\approx 0$.

*Theorem 3:* Under Assumption 1 and Lemma 1, the bias-eliminated estimate $\hat{\mathbf{y}}$ is $\sqrt{M}$-consistent, i.e., $\hat{\mathbf{y}}\approx\mathbf{y}^o$.

*Proof:* The main idea is to analyze and eliminate the asymptotic biases of $\mathbf{H}^\top\mathbf{H}/(MN)$ and $\mathbf{H}^\top\bar{\mathbf{d}}/(MN)$ to approach $\mathbf{H}^{o\top}\mathbf{H}^o/(MN)$ and $\mathbf{H}^{o\top}\bar{\mathbf{d}}^o/(MN)$, respectively. According to Assumption 1 and Lemma 1, we can obtain

$$\frac{\mathbf{H}^\top\mathbf{H}}{MN}\approx\frac{\mathbf{H}^{o\top}\mathbf{H}^o}{MN}+\frac{\mathbf{G}_{a1}}{MN},\quad \frac{\mathbf{H}^\top\bar{\mathbf{d}}}{MN}\approx\frac{\mathbf{H}^{o\top}\bar{\mathbf{d}}^o}{MN}+\frac{\mathbf{G}_{a2}}{MN}. \tag{7}$$

Therefore, $\hat{\mathbf{y}}\approx\hat{\mathbf{y}}^{\mathrm{B}}$. Since $\hat{\mathbf{y}}^{\mathrm{B}}$ in (5) is $\sqrt{M}$-consistent, so is $\hat{\mathbf{y}}$, which completes the proof. The detailed derivation of (7) is shown in Appendix I. ∎

Then, we can recover $\tilde{\mathbf{R}}$ from $\hat{\mathbf{y}}$. Denote the SVD of $\tilde{\mathbf{R}}$ as $\tilde{\mathbf{R}}=\mathbf{U}\mathbf{\Sigma}\mathbf{V}^\top$. The projection of $\tilde{\mathbf{R}}$ onto SO(2) is given by $\hat{\mathbf{R}}=\mathbf{U}\mathrm{diag}([1,\det(\mathbf{U}\mathbf{V}^\top)])\mathbf{V}^\top$. In 3D case, $\hat{\mathbf{R}}=\mathbf{U}\mathrm{diag}([1,1,\det(\mathbf{U}\mathbf{V}^\top)])\mathbf{V}^\top$. As long as $\tilde{\mathbf{R}}$ is $\sqrt{M}$-consistent, so is $\hat{\mathbf{R}}$ [12].

### B. Bias-Eliminated One-Step Gauss-Newton Method

With a consistent estimate as the initial value, we can apply Gauss-Newton iterations to obtain a more precise consistent estimate. However, as stated in Section II, the ML estimate is not necessarily consistent. As a result, applying the Gauss-Newton method directly to the ML problem (3) could lose the consistency of the estimate.

Here, we design a bias-eliminated Gauss-Newton algorithm that is asymptotically equivalent to the Gauss-Newton algorithm applied to the squared-range problem without anchor position uncertainty and thus can retain the consistent property. First, we give the squared-range problem without anchor position uncertainty as follows:

$$\min_{\boldsymbol{\theta},\mathbf{t}}\ \frac{1}{MN}\sum_{i=1}^N\sum_{m=1}^M\left(d_{im}^2-\sigma^2-\|\mathbf{a}_m^o-\mathbf{L}_i\mathrm{vec}\left(\mathbf{R}(\boldsymbol{\theta})\right)-\mathbf{t}\|^2\right)^2, \tag{8}$$

where $\mathbf{L}_i=(\mathbf{s}_i\otimes\mathbf{I}_n)^\top$ and $\mathbf{R}(\boldsymbol{\theta})$ is the rotation matrix induced from the Euler angle vector $\boldsymbol{\theta}$. In 2D case, $\boldsymbol{\theta}$ is a scalar and represents the yaw angle of the rigid body.

*Lemma 2:* Denote the optimal solution to problem (8) as $\hat{\boldsymbol{\theta}}^{\mathrm{SR}}$ and $\hat{\mathbf{t}}^{\mathrm{SR}}$. It holds that $\hat{\boldsymbol{\theta}}^{\mathrm{SR}}\approx\boldsymbol{\theta}^o$ and $\hat{\mathbf{t}}^{\mathrm{SR}}\approx\mathbf{t}^o$.

*Proof:* Set $\mathbf{\Theta}=[\boldsymbol{\theta};\mathbf{t}]$ and $f_{im}^o(\mathbf{\Theta})=\|\mathbf{a}_m^o-\mathbf{L}_i\mathrm{vec}\left(\mathbf{R}(\boldsymbol{\theta})\right)-\mathbf{t}\|$. Then, we have $d_{im}=f_{im}^o(\mathbf{\Theta}^o)+r_{im}$ and

$$(d_{im}^2-\sigma^2-\|\mathbf{a}_m-\mathbf{L}_i\mathrm{vec}\left(\mathbf{R}(\boldsymbol{\theta})\right)-\mathbf{t}\|^2)^2 =$$
$$(f_{im}^o(\mathbf{\Theta})^2-f_{im}^o(\mathbf{\Theta}^o)^2+r_{im}^2+2f_{im}^o(\mathbf{\Theta}^o)r_{im}-\sigma^2)^2.$$

Let $f^o(\mathbf{\Theta})$ and $f^o(\mathbf{\Theta})^2$ denote the sequence $\{f_{im}^o(\mathbf{\Theta})\}_{i,m=1}^{N,M}$ and $\{f_{im}^o(\mathbf{\Theta})^2\}_{i,m=1}^{N,M}$, respectively. From Lemma 1 and Assumption 1, as the anchor number goes to infinity, the objective function in (8) convergences to $\|(f^o(\mathbf{\Theta})^2-f^o(\mathbf{\Theta}^o)^2\|_t^2+c$, where $c$ is a constant.

According to [12], $\|(f^o(\mathbf{\Theta})-f^o(\mathbf{\Theta}^o)\|_t^2$ has a unique minimum at $\mathbf{\Theta}=\mathbf{\Theta}^o$. Note that $f^o(\mathbf{\Theta})\ge 0$ for any $\mathbf{\Theta}$. Hence, $\|(f^o(\mathbf{\Theta})^2-f^o(\mathbf{\Theta}^o)^2\|_t^2$ also has a unique minimum at $\mathbf{\Theta}=\mathbf{\Theta}^o$. As $c$ is a constant, the minimizer of the objective function in (8) converges to $\mathbf{\Theta}^o$, and the convergence speed is $1/\sqrt{M}$ based on Lemma 1. ∎

For the optimization problem shown in (8), we can write its one-step Gauss-Newton iteration as

$$\hat{\mathbf{\Theta}}^{\mathrm{GN}}=\begin{bmatrix}\hat{\boldsymbol{\theta}}\\ \hat{\mathbf{t}}\end{bmatrix}+\left(\frac{\mathbf{J}_T^{o\top}\mathbf{J}_T^o}{MN}\right)^{-1}\left(\frac{\mathbf{J}_T^{o\top}\left(\boldsymbol{\phi}-f^o(\hat{\mathbf{\Theta}})^2\right)}{MN}\right), \tag{9}$$

where $\mathbf{J}_T^o$ denotes the Jacobian matrix for (8), and

$$\boldsymbol{\phi}=\begin{bmatrix}d_{11}^2\\ \vdots\\ d_{NM}^2\end{bmatrix}-\sigma^2\mathbf{1}_{MN}.$$

Based on Lemma 2, the following lemma is straightforward:

*Lemma 3:* The estimate $\hat{\mathbf{\Theta}}^{\mathrm{GN}}$ is $\sqrt{M}$-consistent if the initial value is $\sqrt{M}$-consistent.

For the problem with position uncertainty, we cannot obtain $\mathbf{J}^o$, so we apply a modified one-step Gauss-Newton method shown below:

$$\hat{\mathbf{\Theta}}^{\mathrm{MGN}}=\begin{bmatrix}\hat{\boldsymbol{\theta}}\\ \hat{\mathbf{t}}\end{bmatrix}+\left(\frac{\mathbf{J}_T^\top\mathbf{J}_T-\mathbf{Q}}{MN}\right)^{-1}\left(\frac{\mathbf{J}_T^\top\left(\boldsymbol{\phi}-f(\hat{\mathbf{\Theta}})^2\right)-\mathbf{C}}{MN}\right), \tag{10}$$

where $\mathbf{J}_T$ is the Jacobian matrix for (8) with $\mathbf{a}_m^o$ replaced by $\mathbf{a}_m$, and $\mathbf{Q}$ and $\mathbf{C}$ are the eliminated bias terms, where

$$\mathbf{Q}=\begin{bmatrix}\mathbf{Q}_{11} & \mathbf{Q}_{12}\\ \mathbf{Q}_{21} & \mathbf{Q}_{22}\end{bmatrix},\ \mathbf{Q}_{11}=\sum_{i=1}^N 4M\sigma_a^2(\mathbf{B}_i\mathbf{B}_i^\top),$$
$$\mathbf{Q}_{12}=\sum_{i=1}^N 4M\sigma_a^2 B_i,\ \mathbf{Q}_{21}=\mathbf{Q}_{12}^\top,\ \mathbf{Q}_{12}=4MN\sigma_a^2\mathbf{I}_n.$$
$$\mathbf{C}=\begin{bmatrix}\mathbf{C}_1\\ \mathbf{C}_2\end{bmatrix},\ \mathbf{C}_2=\sum_{i=1}^N\sum_{m=1}^M(2n+4)\sigma_a^2\mathbf{f}_{im}(\hat{\mathbf{\Theta}})$$
$$\mathbf{C}_1=\sum_{i=1}^N\sum_{m=1}^M(2n+4)\sigma_a^2 B_i\mathbf{f}_{im}(\hat{\mathbf{\Theta}}),$$
$$\mathbf{B}_i=\Psi^\top(\mathbf{I}_n\otimes\hat{\mathbf{R}}^\top)\mathbf{L}_i^\top,\Psi=\frac{\partial\mathrm{vec}(\mathbf{R}(0))}{\partial\theta},$$

and $\mathbf{f}_{im}^o(\hat{\mathbf{\Theta}})=\mathbf{a}_m^o-\mathbf{L}_i\mathrm{vec}\left(\hat{\mathbf{R}}\right)-\hat{\mathbf{t}}$ and $\mathbf{f}_{im}(\hat{\mathbf{\Theta}})=\mathbf{f}_{im}^o(\hat{\mathbf{\Theta}})+\boldsymbol{\varepsilon}_m=\mathbf{a}_m-\mathbf{L}_i\mathrm{vec}\left(\hat{\mathbf{R}}\right)-\hat{\mathbf{t}}$.

*Theorem 4:* Under Assumption 1, the estimate $\hat{\mathbf{\Theta}}^{\mathrm{MGN}}$ in (10) is $\sqrt{M}$-consistent if the initial value is $\sqrt{M}$-consistent.

*Proof:* According to Lemma 1, Assumption 1, and the detailed bias-eliminated process described in Appendix II, we can approach $\mathbf{J}_T^{o\top}\mathbf{J}_T^o/(MN)$ and $\mathbf{J}_T^{o\top}(\boldsymbol{\phi} - f^o(\hat{\mathbf{\Theta}})^2)/(MN)$ as follows:

$$\frac{\mathbf{J}_T^\top \mathbf{J}_T}{MN} \approx \frac{\mathbf{J}_T^{o\top}\mathbf{J}_T^o}{MN} + \frac{\mathbf{Q}}{MN},$$
$$\frac{\mathbf{J}_T^\top(\boldsymbol{\phi} - f(\hat{\mathbf{\Theta}})^2)}{MN} \approx \frac{\mathbf{J}_T^{o\top}(\boldsymbol{\phi} - f^o(\hat{\mathbf{\Theta}})^2)}{MN} + \frac{\mathbf{C}}{MN}.$$

This proves that $\hat{\mathbf{\Theta}}^{\mathrm{MGN}} \approx \hat{\mathbf{\Theta}}^{\mathrm{GN}}$. As $\hat{\mathbf{\Theta}}^{\mathrm{GN}}$ is $\sqrt{M}$-consistent (Lemma 3), $\hat{\mathbf{\Theta}}^{\mathrm{MGN}}$ is also $\sqrt{M}$-consistent. ∎

At the end of this section, we summarize our proposed estimator, named Consistent Unconstrained Least Squares refined by a one-step Modified Gauss-Newton iteration (**MGN-CULS**), in Algorithm 1. We then analyze the time complexity of our Algorithm. Line 1 has $O(M)$ (linear) time complexity, Line 2 has $O(1)$ (constant) time complexity, and Line 3 has $O(M)$ (linear) time complexity. Therefore, the whole algorithm has $O(M)$ (linear) time complexity, which is computationally efficient in the large sample case.

**Algorithm 1 MGN-CULS** Estimator

**Input:** $\mathbf{d}$, $\sigma$, $\sigma_a$, $\mathbf{A}$, and $\mathbf{S}$.
**Output:** the estimates of $\mathbf{R}^o$ and $\mathbf{t}^o$.
1: Calculate the **CULS** estimate as (6).
2: Obtain $\tilde{\mathbf{R}}$ and $\hat{\mathbf{t}}$ from the **CULS** estimate and recover $\hat{\mathbf{R}}$ by projecting $\tilde{\mathbf{R}}$ onto $\mathrm{SO}(n)$.
3: Implement the modified one-step Gauss-Newton iteration (10) and obtain the **MGN-CULS** estimate.

## IV. SIMULATION

We design several planar ($n = 2$) simulations to test our algorithm performance. There exist $M$ anchors which are placed randomly in a 100m × 100m room and a rigid body placed at position $\mathbf{t}^o = [5,5]^\top$ and rotation angle $\theta^o = 60^o$. Two tags are mounted on the rigid body at $[10,0]^\top$ and $[10,10]^\top$ in the body frame. Each anchor and tag can communicate multiple times and obtain $T$ measurements.

We run $L = 1000$ Monte-Carlo experiments for each setting to evaluate RMSEs. The RMSEs for the rotation angle and translation vector are given by

$$\mathrm{RMSE}(\hat{\theta}) = \sqrt{\frac{1}{L}\sum_{l=1}^{L}(\hat{\theta}(\omega_l) - \theta^o)^2},$$
$$\mathrm{RMSE}(\hat{\mathbf{t}}) = \sqrt{\frac{1}{L}\sum_{l=1}^{L}\|\hat{\mathbf{t}}(\omega_l) - \mathbf{t}^o\|^2},$$

where $\hat{\theta}(\omega_l)$ and $\hat{\mathbf{t}}(\omega_l)$ is the estimate in the $l$-th Monte-Carlo experiment. We compare our algorithm with previous work including **GTRS** [11], **GN-SDP** [7], **GN-ULS** [12], and **WLS** [13] and also with the lower bound, which is the square root of the trace of CRLB [10], denoted as $\sqrt{CRLB}$. All algorithm simulations are run on an i7-14700K CPU using Matlab.

### A. Simulation 1: Increasing anchor number

In this simulation, we set the number of anchors $M = 3, 10, 100, 1000, 10000$, respectively, and $\sigma = 5$, $\sigma_a = 5$. The RMSE result is shown in Fig. 3, and the computation time result is presented in Fig. 4.

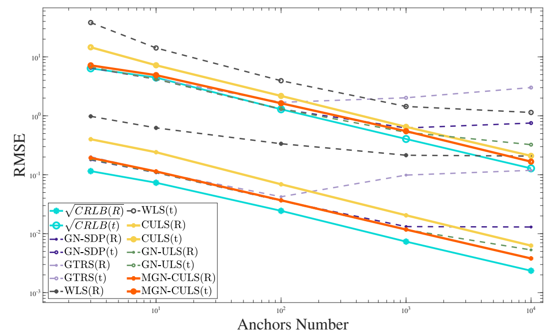


Fig. 3. Performance with numerous anchors.

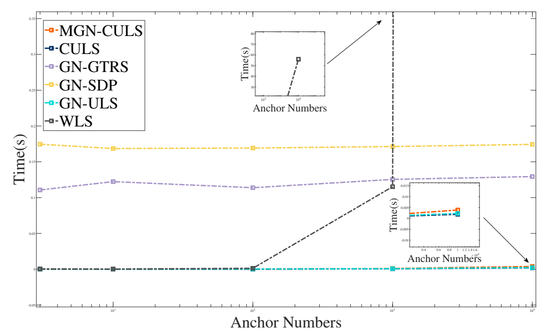


Fig. 4. Time-consuming with numerous anchors.

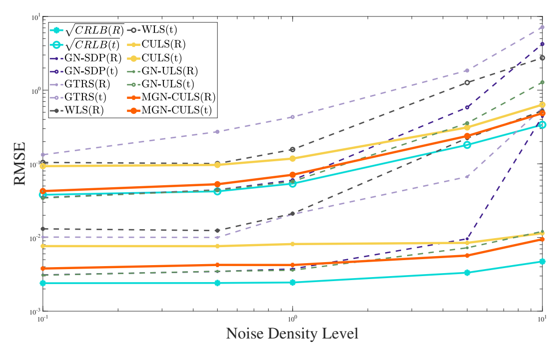


Fig. 5. Performance with different noise level.

Our algorithm is consistent and close to CRLB as the number of anchors increases. Compared with **GN-ULS**, our algorithm has a slightly worse performance when the anchor number is small. However, the **GN-ULS** algorithm is asymptotically biased and has a worse performance when the anchor number increases. Compared with other algorithms, our estimator has better performance in all situations. Our estimator performs well when the anchor number is large because it is asymptotically unbiased. For computation time, our estimator resembles the **GN-ULS** method and is much less than the other methods.

### *B. Simulation 2: Increasing anchor position uncertainty*

In this simulation, we set the anchor number $M = 5000$ and $\sigma_a = 0.1, 0.5, 1, 5, 10$, respectively. The result is shown in Fig. 5. This result shows that our algorithm has a good performance when the noise level is small and has a better performance when the noise level is large compared with other algorithms.

## V. CONCLUSION AND FUTURE WORK

This work studied the pose estimation of a rigid body using range measurements with anchor position uncertainty. We observe that the ML estimate will not converge to the ground truth as the anchor number increases, in other words, the ML estimate is not necessarily consistent. Based on a two-step estimation scheme, we designed an asymptotically unbiased and consistent estimator **MGN-CULS**. Through various simulations, we verify that **MGN-CULS** outperforms existing methods under a large number of measurements and large noise levels and has a relatively low computational complexity. One possible application for this method is estimating a static object's pose using several moving objects. For example, several driving cars with GPS and tags on their bodies will provide an increasing number of distance measurements and positions with uncertainties as time increases. Our method may have better performance in the above situation.

In future work, we want to extend current results in three directions. Firstly, we plan to improve **MGN-CULS**'s performance in the few anchor cases. Secondly, We want to relax the assumption of position uncertainty and consider noises with limited characterization. Last but not least, we plan to fuse range measurements with other sensors to obtain an accurate odometry.

## APPENDIX I
## PROOF FOR THEOREM 3

*Proof:* The proof is based on Lemma 1 and Assumption 1: We can write $\mathbf{H}_1$, $\mathbf{H}_2$ and $\tilde{d}_{im}$ as

$$\begin{aligned}
\mathbf{H}_1 =& -2(\mathbf{I}_N \otimes \mathbf{P})(\mathbf{S}^\top \otimes (\mathbf{A}^o + \boldsymbol{\varepsilon})^\top)\boldsymbol{\Gamma} \\
=& -2(\mathbf{I}_N \otimes \mathbf{P})(\mathbf{S}^\top \otimes \mathbf{A}^{o\top})\boldsymbol{\Gamma} - 2(\mathbf{I}_N \otimes \mathbf{P})(\mathbf{S}^{\top\otimes}\boldsymbol{\varepsilon}^\top)\boldsymbol{\Gamma} \\
=& \mathbf{H}_1^o + \mathbf{r}_{\mathbf{H}1}, \\
\mathbf{H}_2 =& -2(\mathbf{I}_N \otimes \mathbf{P})(\mathbf{1}_N \otimes (\mathbf{A}^o + \boldsymbol{\varepsilon}^\top)) \\
=& -2(\mathbf{I}_N \otimes \mathbf{P})(\mathbf{1}_N \otimes \mathbf{A}^{o\top}) - 2(\mathbf{I}_N \otimes \mathbf{P})(\mathbf{1}_N \otimes \boldsymbol{\varepsilon}^\top) \\
=& \mathbf{H}_2^o + \mathbf{r}_{\mathbf{H}2}. \\
\tilde{d}_{im} =& \tilde{d}_{im}^o - \boldsymbol{\varepsilon}_m{}^\top \boldsymbol{\varepsilon}_m - 2\boldsymbol{\varepsilon}_m{}^\top \mathbf{a}_m^o.
\end{aligned}$$

Then, we have $\tilde{\mathbf{d}} = \tilde{\mathbf{d}}^o - \mathbf{b_A} - \mathbf{e_A}$, where

$$\mathbf{b_A} = \begin{bmatrix} \boldsymbol{\varepsilon}_1^\top \boldsymbol{\varepsilon}_1 \dots \boldsymbol{\varepsilon}_1^\top \boldsymbol{\varepsilon}_1 \\ \vdots \quad \ddots \quad \vdots \\ \boldsymbol{\varepsilon}_m{}^\top \boldsymbol{\varepsilon}_m \dots \boldsymbol{\varepsilon}_m{}^\top \boldsymbol{\varepsilon}_m \end{bmatrix}, \mathbf{e_A} = \begin{bmatrix} 2\boldsymbol{\varepsilon}_1^\top \mathbf{a}_1^o \dots 2\boldsymbol{\varepsilon}_1^\top \mathbf{a}_1^o \\ \vdots \quad \ddots \quad \vdots \\ 2\boldsymbol{\varepsilon}_m{}^\top \mathbf{a}_M^o \dots 2\boldsymbol{\varepsilon}_m{}^\top \mathbf{a}_M^o \end{bmatrix}.$$

We can further obtain

$$\begin{aligned}
\bar{\mathbf{d}} &= (\mathbf{I}_N \otimes \mathbf{P})\,\mathrm{vec}(\tilde{\mathbf{d}}) \\
&= \bar{\mathbf{d}}^o - (\mathbf{I}_N \otimes \mathbf{P})(\mathbf{1}_N \otimes \mathbf{b}_{\mathbf{A}1}) - (\mathbf{I}_N \otimes \mathbf{P})(\mathbf{1}_N \otimes \mathbf{e}_{\mathbf{A}1}),
\end{aligned}$$

where

$$\mathbf{b}_{\mathbf{A}1} = \begin{bmatrix} \boldsymbol{\varepsilon}_1^\top \boldsymbol{\varepsilon}_1 \\ \vdots \\ \boldsymbol{\varepsilon}_m{}^\top \boldsymbol{\varepsilon}_m \end{bmatrix} = n\sigma_a^2 \mathbf{1}_M, \quad \mathbf{e}_{\mathbf{A}1} = \begin{bmatrix} 2\boldsymbol{\varepsilon}_1^\top \mathbf{a}_1^o \\ \vdots \\ 2\boldsymbol{\varepsilon}_m{}^\top \mathbf{a}_M^o \end{bmatrix}.$$

Therefore, according to Lemma 1 and Assumption 1, we have

$$\begin{aligned}
\frac{\mathbf{H}_1^\top \mathbf{H}_1}{MN} &= \frac{\mathbf{H}_1^{o\top} \mathbf{H}_1^o}{MN} + \frac{\mathbf{r}_{\mathbf{H}_1}^\top \mathbf{r}_{\mathbf{H}_1}}{MN} \\
&\approx \frac{\mathbf{H}_1^{o\top} \mathbf{H}_1^o}{MN} + \frac{4\boldsymbol{\Gamma}^\top (\mathbf{S}\mathbf{S}^\top \otimes \boldsymbol{\varepsilon}\mathbf{P}\boldsymbol{\varepsilon}^\top)\boldsymbol{\Gamma}}{MN} \\
&\approx \frac{\mathbf{H}_1^{o\top} \mathbf{H}_1^o}{MN} + 4KM\sigma_a^2 \Gamma^\top (\mathbf{S}\mathbf{S}^\top \otimes \mathbf{I}_n)\Gamma. \\
\frac{\mathbf{H}_2^\top \mathbf{H}_2}{MN} &= \frac{\mathbf{H}_2^{o\top} \mathbf{H}_2^o}{MN} + \frac{\mathbf{r}_{\mathbf{H}_2}^\top \mathbf{r}_{\mathbf{H}_2}}{MN} \\
&\approx \frac{\mathbf{H}_2^{o\top} \mathbf{H}_2^o}{MN} + \frac{4(\mathbf{1}_N^\top \mathbf{1}_N \otimes \boldsymbol{\varepsilon}\mathbf{P}\boldsymbol{\varepsilon}^\top)}{MN} \\
&\approx \frac{\mathbf{H}_2^{o\top} \mathbf{H}_2^o}{MN} + 4KMN{\sigma_a}^2 \mathbf{I}_n.
\end{aligned}$$

$$\begin{aligned}
\frac{\mathbf{H}_1^\top \mathbf{H}_2}{MN} &= \frac{\mathbf{H}_1^{o\top} \mathbf{H}_2^o}{MN} + \frac{\mathbf{r}_{\mathbf{H}_1}^\top \mathbf{r}_{\mathbf{H}_2}}{MN} \\
&\approx \frac{\mathbf{H}_1^{o\top} \mathbf{H}_2^o}{MN} + \frac{4\boldsymbol{\Gamma}^\top (\mathbf{S}\mathbf{1}_N \otimes \boldsymbol{\varepsilon}\mathbf{P}\boldsymbol{\varepsilon}^\top)}{MN} \\
&\approx \frac{\mathbf{H}_1^{o\top} \mathbf{H}_2^o}{MN} + \frac{4KM\sigma_a^2 \boldsymbol{\Gamma}^\top (\mathbf{S}\mathbf{1}_N \otimes \mathbf{I}_n)}{MN}. \\
\frac{\mathbf{H}_1^\top \bar{\mathbf{d}}}{MN} &\approx \frac{\mathbf{H}_1^{o\top} \bar{\mathbf{d}}^o}{MN} + \frac{4\boldsymbol{\Gamma}^\top (\mathbf{S} \otimes \boldsymbol{\varepsilon})(\mathbf{I}_N \otimes \mathbf{P})(\mathbf{1}_N \otimes \mathbf{e}_{\mathbf{A}1})}{MN} \\
&\approx \frac{\mathbf{H}_1^{o\top} \bar{\mathbf{d}}^o}{MN} + \frac{4\boldsymbol{\Gamma}^\top (\mathbf{S}\mathbf{1}_N \otimes \boldsymbol{\varepsilon}\mathbf{P}\mathbf{e}_{\mathbf{A}1})}{MN} \\
&\approx \frac{\mathbf{H}_1^{o\top} \bar{\mathbf{d}}^o}{MN} + \frac{4K{\sigma_a}^2 \boldsymbol{\Gamma}^\top (\mathbf{S}\mathbf{1}_N \otimes \mathbf{A}\mathbf{1}_M)}{MN}.
\end{aligned}$$

$$\begin{aligned}
\frac{\mathbf{H}_2^\top \bar{\mathbf{d}}}{MN} &\approx \frac{\mathbf{H}_2^{o\top} \bar{\mathbf{d}}^o}{MN} + \frac{4(\mathbf{1}_N^\top \otimes \boldsymbol{\varepsilon})(\mathbf{I}_N \otimes \mathbf{P})(\mathbf{1}_N \otimes \mathbf{e}_{\mathbf{A}1})}{MN} \\
&\approx \frac{\mathbf{H}_2^{o\top} \bar{\mathbf{d}}^o}{MN} + \frac{4(\mathbf{1}_N^\top \mathbf{1}_N \otimes \boldsymbol{\varepsilon}\mathbf{P}\mathbf{e}_{\mathbf{A}1})}{MN} \\
&\approx \frac{\mathbf{H}_2^{o\top} \bar{\mathbf{d}}^o}{MN} + \frac{4KN{\sigma_a}^2 \mathbf{A}\mathbf{1}_M}{MN}.
\end{aligned}$$

■

## APPENDIX II
## PROOF FOR THEOREM 4

*Proof:* Set

$$\begin{aligned}
\mathbf{J} = \begin{bmatrix} \mathbf{J}_1 \\ \mathbf{J}_2 \end{bmatrix} &= \frac{\partial f_{im}(\hat{\boldsymbol{\Theta}})^2}{\partial(\hat{\boldsymbol{\theta}}, \hat{\mathbf{t}})} = \begin{bmatrix} -2\mathbf{B}_i(\mathbf{f}_{im}^o(\hat{\boldsymbol{\Theta}}) + \boldsymbol{\varepsilon}_m) \\ -2(\mathbf{f}_{im}^o(\hat{\boldsymbol{\Theta}}) + \boldsymbol{\varepsilon}_m) \end{bmatrix}^\top. \\
f_{im}(\hat{\boldsymbol{\Theta}})^2 &= f_{im}^o(\hat{\boldsymbol{\Theta}})^2 + \boldsymbol{\varepsilon}_m{}^\top \boldsymbol{\varepsilon}_m + 2\mathbf{f}_{im}^o(\hat{\boldsymbol{\Theta}})^\top \boldsymbol{\varepsilon}_m.
\end{aligned}$$

For term $\mathbf{J}^\top\mathbf{J}$, textcolorredaccording to Assumption 1, we have equations below:

$$\begin{aligned}
\frac{\mathbf{J}_1^\top\mathbf{J}_1}{MN} &= \frac{4\mathbf{B}_i(\mathbf{f}_{im}^o(\hat{\mathbf{\Theta}})+\boldsymbol{\varepsilon}_m)(\mathbf{f}_{im}^o(\hat{\mathbf{\Theta}})+\boldsymbol{\varepsilon}_m)^\top\mathbf{B}_i^\top}{MN} \\
&\approx \frac{4\mathbf{B}_i(\mathbf{f}_{im}^o(\hat{\mathbf{\Theta}}))(\mathbf{f}_{im}^o(\hat{\mathbf{\Theta}}))^\top\mathbf{B}_i^\top}{MN} + \frac{4\mathbf{B}_i\boldsymbol{\varepsilon}_m\boldsymbol{\varepsilon}_m^\top\mathbf{B}_i^\top}{MN} \\
&\approx \frac{\mathbf{J}_1^{o\top}\mathbf{J}_1^o}{MN} + \frac{4\sigma_a^2(\mathbf{B}_i\mathbf{B}_i^\top)}{MN}. \\
\frac{\mathbf{J}_2^\top\mathbf{J}_2}{MN} &= \frac{4(\mathbf{f}_{im}^o(\hat{\mathbf{\Theta}})+\boldsymbol{\varepsilon}_m)(\mathbf{f}_{im}^o(\hat{\mathbf{\Theta}})+\boldsymbol{\varepsilon}_m)^\top}{MN} \\
&\approx \frac{4(\mathbf{f}_{im}^o(\hat{\mathbf{\Theta}}))(\mathbf{f}_{im}^o(\hat{\mathbf{\Theta}}))^\top}{MN} + \frac{4\boldsymbol{\varepsilon}_m\boldsymbol{\varepsilon}_m^\top}{MN} \\
&\approx \frac{\mathbf{J}_2^{o\top}\mathbf{J}_2^o}{MN} + \frac{4\sigma_a^2\mathbf{I}_n}{MN}. \\
\frac{\mathbf{J}_1^\top\mathbf{J}_2}{MN} &= \frac{4\mathbf{B}_i(\mathbf{f}_{im}^o(\hat{\mathbf{\Theta}})+\boldsymbol{\varepsilon}_m)(\mathbf{f}_{im}^o(\hat{\mathbf{\Theta}})+\boldsymbol{\varepsilon}_m)^\top}{MN} \\
&\approx \frac{4\mathbf{B}_i(\mathbf{f}_{im}^o(\hat{\mathbf{\Theta}}))(\mathbf{f}_{im}^o(\hat{\mathbf{\Theta}}))^\top}{MN} + \frac{4\mathbf{B}_i\boldsymbol{\varepsilon}_m\boldsymbol{\varepsilon}_m^\top}{MN} \\
&\approx \frac{\mathbf{J}_1^{o\top}\mathbf{J}_2^o}{MN} + \frac{4\sigma_a^2\mathbf{B}_i}{MN}.
\end{aligned}$$

For $\mathbf{J}^\top(\boldsymbol{\phi}-f_{im}(\hat{\mathbf{\Theta}})^2)$ we have:

$$\mathbf{J}_1^\top\boldsymbol{\phi}\approx\mathbf{J}_1^{o\top}\boldsymbol{\phi} \quad\text{and,}\quad \mathbf{J}_2^\top\boldsymbol{\phi}\approx\mathbf{J}_2^{o\top}\boldsymbol{\phi}.$$

$$\begin{aligned}
\frac{\mathbf{J}_1^\top f_{im}(\hat{\mathbf{\Theta}})^2}{MN} &= -2\mathbf{B}_i(\mathbf{f}_{im}^o(\hat{\mathbf{\Theta}})+\boldsymbol{\varepsilon}_m) \\
&\quad \frac{(f_{im}^o(\hat{\mathbf{\Theta}})^2+\boldsymbol{\varepsilon}_m{}^\top\boldsymbol{\varepsilon}_m+2\mathbf{f}_{im}^o(\hat{\mathbf{\Theta}})^\top\boldsymbol{\varepsilon}_m)}{MN} \\
&= -\frac{2\mathbf{B}_i(\mathbf{f}_{im}^o(\hat{\mathbf{\Theta}}))f_{im}^o(\hat{\mathbf{\Theta}})^o}{MN} - \frac{2\mathbf{B}_i(\mathbf{f}_{im}^o(\hat{\mathbf{\Theta}}))\boldsymbol{\varepsilon}_m^\top\boldsymbol{\varepsilon}_m}{MN} \\
&\quad -\frac{4\mathbf{B}_i(\mathbf{f}_{im}^o(\hat{\mathbf{\Theta}}))(\mathbf{f}_{im}^o(\hat{\mathbf{\Theta}}))^\top\boldsymbol{\varepsilon}_m}{MN} - \frac{2\mathbf{B}_i\boldsymbol{\varepsilon}_m f_{im}^o(\hat{\mathbf{\Theta}})^2}{MN} \\
&\quad -\frac{2\mathbf{B}_i\boldsymbol{\varepsilon}_m\boldsymbol{\varepsilon}_m^\top\boldsymbol{\varepsilon}_m}{MN} - \frac{4\mathbf{B}_i\boldsymbol{\varepsilon}_m(\mathbf{f}_{im}^o(\hat{\mathbf{\Theta}}))^\top\boldsymbol{\varepsilon}_m}{MN} \\
&\approx \frac{\mathbf{J}_1^{o\top}f_{im}^o(\hat{\mathbf{\Theta}})^2}{MN} - \frac{2n\sigma_a^2\mathbf{f}_{im}(\hat{\mathbf{\Theta}})}{MN} - \frac{4\mathbf{B}_i\sigma_a^2\mathbf{f}_{im}(\hat{\mathbf{\Theta}})}{MN} \\
&\approx \frac{\mathbf{J}_1^{o\top}f_{im}^o(\hat{\mathbf{\Theta}})^2}{MN} - \frac{(2n+4)\mathbf{B}_i\sigma_a^2\mathbf{f}_{im}(\hat{\mathbf{\Theta}})}{MN}.
\end{aligned}$$

$$\begin{aligned}
\mathbf{J}_2^\top\mathbf{f}_{im}(\hat{\mathbf{\Theta}}) &= -2(\mathbf{f}_{im}^o(\hat{\mathbf{\Theta}})+\boldsymbol{\varepsilon}_m) \\
&\quad \frac{(\mathbf{f}_{im}^o(\hat{\mathbf{\Theta}})+\boldsymbol{\varepsilon}_m{}^\top\boldsymbol{\varepsilon}_m+2\mathbf{f}_{im}^o(\hat{\mathbf{\Theta}})^\top\boldsymbol{\varepsilon}_m)}{MN} \\
&= -\frac{2(\mathbf{f}_{im}^o(\hat{\mathbf{\Theta}}))\mathbf{f}_{im}^o(\hat{\mathbf{\Theta}})}{MN} - \frac{2(\mathbf{f}_{im}^o(\hat{\mathbf{\Theta}}))\boldsymbol{\varepsilon}_m^\top\boldsymbol{\varepsilon}_m}{MN} \\
&\quad -\frac{4(\mathbf{f}_{im}^o(\hat{\mathbf{\Theta}}))(\mathbf{f}_{im}^o(\hat{\mathbf{\Theta}}))^\top\boldsymbol{\varepsilon}_m}{MN} - \frac{2\boldsymbol{\varepsilon}_m\mathbf{f}_{im}^o(\mathbf{\Theta})}{MN} \\
&\quad -\frac{2\boldsymbol{\varepsilon}_m\boldsymbol{\varepsilon}_m^\top\boldsymbol{\varepsilon}_m}{MN} - \frac{4\boldsymbol{\varepsilon}_m(\mathbf{f}_{im}^o(\hat{\mathbf{\Theta}}))^\top\boldsymbol{\varepsilon}_m}{MN} \\
&\approx \frac{\mathbf{J}_1^{o\top}f_{im}^o(\hat{\mathbf{\Theta}})^2}{MN} - \frac{2n\sigma_a^2\mathbf{f}_{im}(\hat{\mathbf{\Theta}})}{MN} - \frac{4\sigma_a^2\mathbf{f}_{im}(\hat{\mathbf{\Theta}})}{MN} \\
&\approx \frac{\mathbf{J}_1^{o\top}f_{im}^o(\hat{\mathbf{\Theta}})^2}{MN} - \frac{(2n+4)\sigma_a^2 f_{im}(\hat{\mathbf{\Theta}})}{MN}.
\end{aligned}$$

■


## Acknowledgement

This work was supported in part by the National Natural Science Foundation of China under Grant 62273288, 62336005, 62273223, and 62122026, in part by Shenzhen Science and Technology Program JCYJ20220818103000001, and in part by the Project of Science and Technology Commission of Shanghai Municipality under Grant 22JC1401401.


## References


[1] X. Ke, Y. Wang, and L. Huang, "Three-dimensional rigid body localization in the presence of clock offsets," *IEEE Signal Processing Letters*, vol. 27, pp. 96–100, 2020.

[2] G. Michieletto, A. Cenedese, and A. Franchi, "Bearing rigidity theory in se (3)," in *2016 IEEE 55th Conference on Decision and Control (CDC)*. IEEE, 2016, pp. 5950–5955.

[3] B. Yi, C. Jin, L. Wang, G. Shi, and I. R. Manchester, "An almost globally convergent observer for visual slam without persistent excitation," in *2021 60th IEEE Conference on Decision and Control (CDC)*. IEEE, 2021, pp. 5441–5446.

[4] Y. Song, M. Guan, W. P. Tay, C. L. Law, and C. Wen, "Uwb/lidar fusion for cooperative range-only slam," in *2019 international conference on robotics and automation (ICRA)*. IEEE, 2019, pp. 6568–6574.

[5] E. Marchand, H. Uchiyama, and F. Spindler, "Pose estimation for augmented reality: a hands-on survey," *IEEE transactions on visualization and computer graphics*, vol. 22, no. 12, pp. 2633–2651, 2015.

[6] N. Funabiki, B. Morrell, J. Nash, and A.-a. Agha-mohammadi, "Range-aided pose-graph-based slam: Applications of deployable ranging beacons for unknown environment exploration," *IEEE Robotics and Automation Letters*, vol. 6, no. 1, pp. 48–55, 2020.

[7] J. Jiang, G. Wang, and K. Ho, "Accurate rigid body localization via semidefinite relaxation using range measurements," *IEEE Signal Processing Letters*, vol. 25, no. 3, pp. 378–382, 2017.

[8] B. Hao, K. Ho, and Z. Li, "Range-based rigid body localization with a calibration emitter for mitigating anchor position uncertainties," *IEEE Transactions on Wireless Communications*, vol. 18, no. 12, pp. 5734–5748, 2019.

[9] X. Wu, Q. Lin, and H. Qi, "Cooperative multiple rigid body localization via semidefinite relaxation using range measurements," *IEEE Transactions on Signal Processing*, vol. 70, pp. 4788–4803, 2022.

[10] S. P. Chepuri, G. Leus, and A.-J. van der Veen, "Rigid body localization using sensor networks," *IEEE Transactions on Signal Processing*, vol. 62, no. 18, pp. 4911–4924, 2014.

[11] S. Chen and K. C. Ho, "Accurate localization of a rigid body using multiple sensors and landmarks," *IEEE Transactions on Signal Processing*, vol. 63, no. 24, pp. 6459–6472, 2015.

[12] H. Jiang, W. Wang, Y. Shen, X. Li, X. Ren, B. Mu, and J. Wu, "Efficient planar pose estimation via uwb measurements," in *2023 IEEE International Conference on Robotics and Automation (ICRA)*, 2023, pp. 1954–1960.

[13] Z. Ma and K. Ho, "Toa localization in the presence of random sensor position errors," in *2011 IEEE International Conference on Acoustics, Speech and Signal Processing (ICASSP)*. IEEE, 2011, pp. 2468–2471.

[14] Y. Gan, X. Cong, and Y. Sun, "Refinement of toa localization with sensor position uncertainty in closed-form," *Sensors*, vol. 20, no. 2, p. 390, 2020.

[15] Y. Zou and Q. Wan, "Asynchronous time-of-arrival-based source localization with sensor position uncertainties," *IEEE Communications Letters*, vol. 20, no. 9, pp. 1860–1863, 2016.

[16] G. Yang, Y. Yan, H. Wang, and X. Shen, "Improved robust toa-based source localization with individual constraint of sensor location uncertainty," *Signal Processing*, vol. 196, p. 108504, 2022.

[17] Z. W. Mekonnen and A. Wittneben, "Robust toa based localization for wireless sensor networks with anchor position uncertainties," *2014 IEEE 25th Annual International Symposium on Personal, Indoor, and Mobile Radio Communication (PIMRC)*, pp. 2029–2033, 2014.

[18] G. Zeng, Q. Zeng, X. Li, B. Mu, J. Chen, L. Shi, and J. Wu, "Consistent and asymptotically statistically-efficient solution to camera motion estimation," *arXiv preprint arXiv:2403.01174*, 2024.

[19] G. Zeng, B. Mu, J. Chen, Z. Shi, and J. Wu, "Global and asymptotically efficient localization from range measurements," *IEEE Transactions on Signal Processing*, vol. 70, pp. 5041–5057, 2022.